

Content from this work may be used under the terms of the CC BY 3.0 licence (© 2019). Any distribution of this work must maintain attribution to the author(s), title of the work, publisher, and DOI.

DEVELOPMENT OF SUPERCONDUCTING QUARTER-WAVE RESONATOR AND CRYOMODULE FOR LOW-BETA ION ACCELERATORS AT RIKEN RADIOACTIVE ISOTOPE BEAM FACTORY

N. Sakamoto*, T. Dantsuka, M. Fujimaki, H. Imao, O. Kamigaito, K. Kusaka, H. Okuno, K. Ozeki, K. Suda, A. Uchiyama, T. Watanabe, Y. Watanabe, K. Yamada
RIKEN Nishina Center, Saitama, Japan
E. Kako, H. Nakai, H. Sakai, K. Umemori, KEK, Ibaraki, Japan
H. Hara, A. Miyamoto, K. Sennyu, T. Yanagisawa
Mitsubishi Heavy Industries Machinery Systems, Ltd. (MHI-MS), Hyogo, Japan

Abstract

A prototype cryomodule with a superconducting quarter-wave resonator (SC-QWR) has been developed at RIKEN Radioactive Isotope Beam Factory (RIBF). During the last SRF conference, we presented the performance of our first SC-QWR and the first cool-down test of its cryomodule. Since then, we have continued our efforts to improve cavity performance and succeeded in recovering deteriorated Q_0 . In this paper, we report what we constructed and learned from the prototype, including design issues with the cavity and its cryomodule. Design issues related to the new SC-QWRs and their cryomodules for the SC linac booster of the RIKEN Heavy-Ion Linac (RILAC) are described as well.

INTRODUCTION

RIBF [1] is a cyclotron-based accelerator facility combined with the heavy ion linac injectors RILAC (RIKEN Linear Accelerator) [2] and RILAC2 [3]. At the RIBF, heavy-ion beams of varying energy are available, ranging from sub-coulomb energy levels for fusion reactions to intermediate energy levels for radioisotope beam production using fission reactions. Beams of ion species ranging from hydrogen to uranium are accelerated to various energies in accordance with experimental requirements.

Design work on the SC linac started with the idea of obtaining a much more intense uranium beam, with an intensity of up to $1 \text{ p}\mu\text{A}$, by introducing a new linac injector [4]. The SC part of the new injector, which consists of 14 cryomodules each containing 4 TEM-mode SC-QWRs, accelerates an $1 \text{ mA } ^{238}\text{U}^{35+}$ beam to 11 MeV/u . The SC-QWR produces a 1.4 MV gap voltage for $\beta = 0.08$ particles at an RF frequency of 73.0 MHz in the continuum wave (CW) mode.

Since 2015, the accelerator group of Nishina Center has joined the ImPACT program [5], led by Dr. Fujita, to develop a system for processing so-called long-lived fission products (LLFPs) via nuclear reactions and transmutations induced by high-intensity ion beams provided by a particle accelerator [6]. As part of this program, a prototype SC linac has been developed. The main purpose of this prototype is to achieve a high acceleration field gradient E_{acc} with a low power dissipation SC cavity, that is, a high- Q_0 and

spatially efficient cryomodule. The cryomodule is the main component of the SC linac, which comprises 4 K SC cavities. Finally, we attempted to assess the stability and reliability of the accelerating field using the prototype cryomodule since reliability of the accelerator is one of the critical issues to avoid a serious impact to the target system.

The prototype cryomodule (Fig. 1) consists of one SC cavity, one dummy cavity, and a vacuum vessel equipped with a 40 K thermal shield cooled by a cryocooler. The

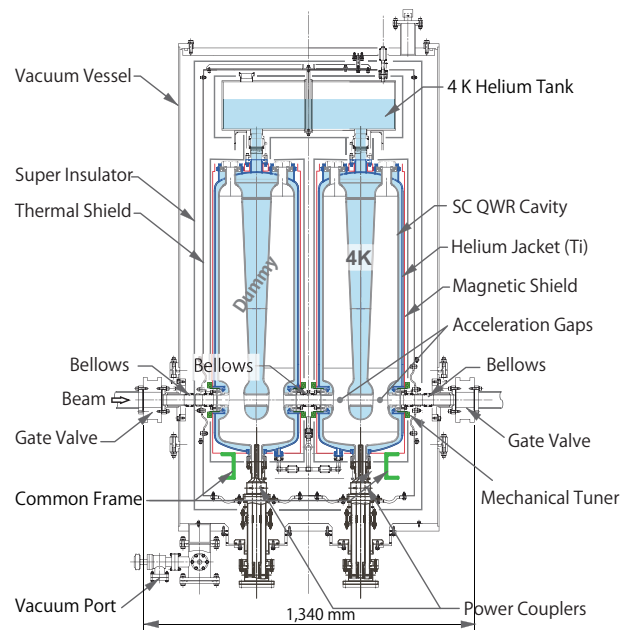


Figure 1: Schematic of prototype cryomodule.

developed SC-QWR is based on the structure of a coaxial resonator with the quarter-wave length with an optimum β as low as 0.08 and a resonant frequency of 75.5 MHz . The SC-QWR is equipped with a cold frequency tuner that can change the resonance up to 6 kHz . The planned operating E_{acc} is 4.5 MV/m with a Q_0 of 8.9×10^8 [6], which is estimated by using the 3D simulation package Micro Wave Studio (MWS) [7]. The cavity's Q -factor became worse each time vertical tests (VTs) were performed, as reported in SRF'17 [8]. After a Q -factor of 8.6×10^8 was observed at the VT2, the Q -factors were decreased to as small as 5×10^8 at VT3 and VT4, which was 50% of our target value.

* nsakamot@ribf.riken.jp

To understand these phenomena, we studied the prototype cavity extensively after the conference. We disassembled the cavity from the prototype cryomodule and succeeded in recovering the cavity performance by removing the defects which deteriorate the cavity performance. Then, the cavity was incorporated into the prototype cryomodule again, and the cool-down test and RF test were performed. In the RF test, the newly developed digital low level RF (LLRF) control was used.

In 2016, it was decided that the total acceleration voltage of the RILAC would be upgraded to allow studies of super-heavy elements aimed at new super-heavy element synthesis. In this upgrade project, a new SC electron cyclotron resonance (ECR) ion source and SC booster linac are being developed and constructed. The SC linac consists of 10 QWRs that are operated at 73.0 MHz and contained in three cryomodules. The basic design of the cavity and its cryomodule differs from that of the 75.5 MHz prototype.

DEVELOPMENT OF SC-QWR

Study of Cavity Performance

At RIKEN, two types of QWRs have been developed so far. A prototype SC-QWR with a frequency of 75.5 MHz was developed under the ImpACT program. The other, a 73.0 MHz QWR, was developed for the RILAC upgrade. The specifications of these cavities are summarized in Table 1. In this table, R/Q , $E_{\text{peak}}/E_{\text{acc}}$, and $B_{\text{peak}}/E_{\text{acc}}$ are esti-

Table 1: Cavity Specifications

SC-QWR		Prototype	SRILAC
Frequency@4 K	[MHz]	75.5	73.0
Temperature	[K]	4	
Height	[mm]	1055	1103
L_{cav}	[mm]	318	320
β_{opt}		0.08	
$E_{\text{peak}}/E_{\text{acc}}$		6.0	6.2
$B_{\text{peak}}/E_{\text{acc}}$	[mT/(MV/m)]	9.5	9.6
R/Q	[Ω]	578	579
G	[Ω]	23.5	22.4
V_{acc}	[MV]	1.4	2.2
E_{acc}	[MV/m]	4.5	6.8
$Q_0 @ E_{\text{acc}}$		2.3×10^9	3.4×10^9
$P_0 @ E_{\text{acc}}$	[W]	1.5	2.4
Q_{pickup}		2.8×10^{11}	1.0×10^{11}

mated by 3D simulation with MWS, and the measured Q_0 , Q_{pickup} are listed. Both of these cavities were fabricated from pure niobium sheets with their RRR of 250 provided by Tokyo Denkai Co., Ltd. (TD). For the port flanges, hard pure (grade 2) niobium, provided by ULVAC, Inc. is used, and a tin-plated metal o-ring (U-TIGHTSEAL), provided by USUI Co., Ltd., is employed.

As a baseline process of surface treatment, buffered chemical polishing (BCP) was chosen, following a fairly standard and widely used procedure. The process was performed via

the following steps: (1) bulk etching ($\sim 100 \mu\text{m}$) by BCP, (2) degassing (750°C , 3hr) by a vacuum furnace, light etching ($\sim 20 \mu\text{m}$) by BCP, (3) rinsing with ultrapure water emitted from a sapphire nozzle with high pressure scanning the inner surface, (4) 120°C , 48 h baking. BCP utilizes an acid mixture in the volumetric proportion $\text{HF}:\text{HNO}_3:\text{H}_3\text{PO}_4 = 1:1:2$. The BCP facility [9] is a circulation system with temperature control, whereby the inlet temperature is maintained at around 15°C , while the returning liquid temperature reaches about 25°C . The average etching rate was $1.1 \mu\text{m}/\text{min}$. In order to polish as uniform as possible, etching was performed in both upright and inverse positions. While the frequency shift rate was estimated to be $0.1 \text{ kHz}/\mu\text{m}$ by simulations with MWS, the actual rate was $0.2 \text{ kHz}/\mu\text{m}$.

The prototype 75.5 MHz cavity is equipped with a pair of test ports along the perpendicular to the beam ports (Fig. 2(A)). As mentioned above, Q_0 dropped to as low as 50% of the target value at VT4. During VT4, heavy multipacting occurred. At the same time, a temperature rise was detected by a temperature sensor installed on the blank flange for the side test port. After disassembling the cryomodule, the prototype cavity was carefully examined and some discharge marks were found on the surface of the vacuum seal (Fig. 2(B)). Also, it appeared like tin that peeled off from the vacuum seal adhered to the surfaces of the test port flanges, as shown in Fig. 2(C).

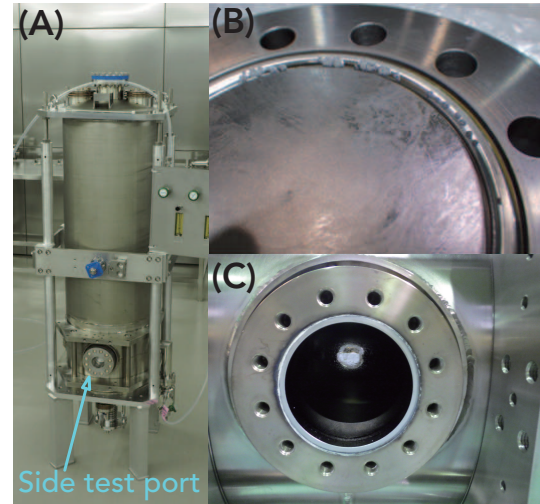


Figure 2: (A) Picture of the prototype cavity. A niobium plug was installed to the side test ports for VT6. (B) Side test port flange. (C) Blank flange with a metal vacuum seal for the side test port.

After cleaning the flanges and replacing the vacuum seals, VT5 was performed. Then, a Q_0 value of 2.3×10^9 , which was four times that of VT4, was achieved. Measured Q_0 is plotted as a function of E_{acc} in Fig. 3.

It is generally reported that surface polishing based by BCP results in a rather steep Q slope at high E_{acc} . As shown in Fig. 3, the Q_0 for the prototype cavity starts to decrease at around $7 \text{ MV}/\text{m}$, yet the performance exceeds our target value of 8.6×10^8 at $4.5 \text{ MV}/\text{m}$ by a large margin.

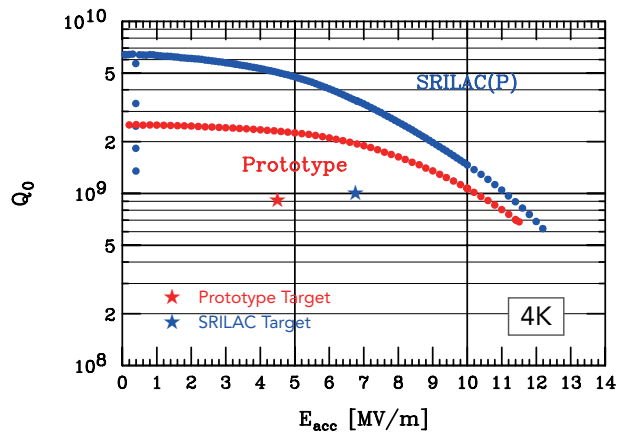


Figure 3: Measured Q_0 versus E_{acc} . The red solid circles represent the measurements conducted in VT5 for the prototype cavity. The blue solid circles are for the SRILAC cavity.

Study of Frequency Tuning

Frequency tuning during fabrication is time-consuming in the case of low-beta structure cavities [10]. Since a mechanical frequency tuner operating at liquid helium temperatures is difficult to make the resonant frequency lower by more than 10 kHz, the error of the cavity frequency referring to the operational frequency has to be between +0 and +10 kHz. There is the possibility of adjusting the frequency during the fabrication process. During welding processes, the lengths of the straight section of the upper and bottom parts are adjusted by measuring the resonance of the temporarily assembled cavity. During the BCP process, the amount of etching can be chosen according to the frequency. Nevertheless, a careful tuning was performed, since it is difficult to estimate the frequency shift caused by shrinkage due to welding-induced shrinkage, annealing-induced deformation, jacketing, pumping, cooling, etc., the error in the total frequency shift can be assumed to be as large as several tens of kilohertz.

One effective way of frequency tuning is differential etching [11]. The structure of QWR is based on a coaxial line and the top and bottom parts of the QWR correspond to the short and open ends, respectively. If the open (short) end is removed, the capacitance (inductance) of the resonant circuit is decreased (increased) and the frequency increases (decreases). The frequency shift was estimated by MWS simulations, as indicated in Fig. 4. The amount of the shift has a maximum at some medium level, as expected.

To verify the estimation (Fig. 4), differential etching was performed in an upright position. Etching liquid was supplied from one of the bottom ports and returned through a pipe inserted into the other bottom port. It resembles an aquarium overflow system. In practice, the etching liquid level can be determined by the insertion length of the return pipe. The differential etching level was set to $h = 580.8$ mm. After the differential etching, a uniform etching with an amount of $26.2 \mu\text{m}$ was performed. It was estimated

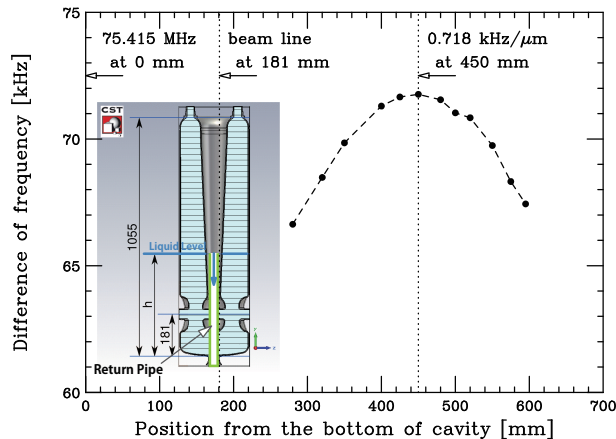


Figure 4: Frequency shift estimated by MWS simulations as a function of etching level from bottom of cavity.

the differential etching of $26 \mu\text{m}$ increased the frequency by 12.6 kHz at 4 K. The shift rate $0.5 \text{ kHz}/\mu\text{m}$ is consistent with the estimation (Fig. 4), while the estimated shift rate of uniform etching was twice the estimated value.

As an alternative frequency tuning method, we try to investigate the effect of the plug tuner. It is expected that a pair of plug tuners, machined to high precision and inserted into the test port, will yield a target frequency within several kilohertz. The frequency shift is calculated as a function of the insertion length of the pair of plug tuners in Fig. 5. The plug tuner block was made of niobium with an RRR

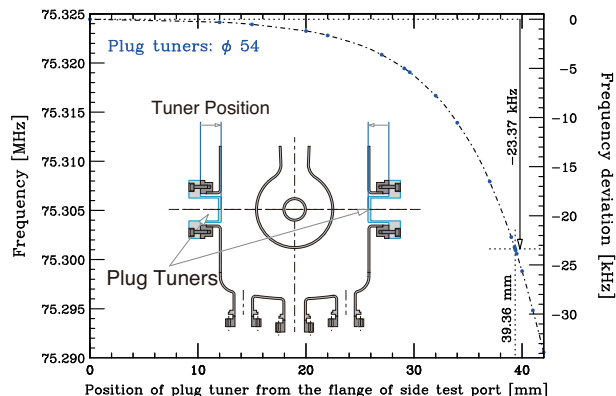


Figure 5: Frequency shift estimated by MWS simulations versus the insertion length of the pair of plug tuners.

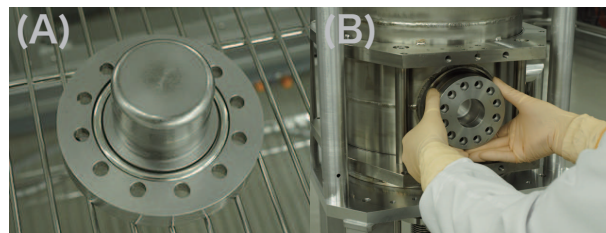


Figure 6: (A) Plug tuner block machined from pure niobium (RRR = 250) welded to a flange made of Grade 2 niobium. (B) Installation of a plug tuner.

Content from this work may be used under the terms of the CC BY 3.0 licence (© 2019). Any distribution of this work must maintain attribution to the author(s), title of the work, publisher, and DOI.

of 250. In Fig. 6, photos of the plug tuner itself (A) and installation (B) are shown. After the installation, VT6 was performed. The frequency shift observed was 27.2 kHz, while the expected value was 23.4 kHz. It was found that Q_0 unexpectedly deteriorated, dropping to roughly one-tenth its value measured at VT5.

Design Feedback to the SRILAC Cavity

The specifications of the cavity for the SRILAC are summarized in Table 1. Since the effect of the side test ports on cavity performance seems rather large, the cavity for the SRILAC was not equipped with side test ports. On the basis of the results of VTs on the prototype cavity, the target Q_0 was set 1×10^9 to E_{acc} 6.8 MV/m. The measured Q_0 of the SRILAC prototype is plotted in Fig. 3 together with the Q_0 of the 75.5 MHz prototype cavity. We achieved a high performance with the cavity for the SRILAC, whose Q_0 exceeded the target value by a large margin. Though differential BCP is effective for frequency tuning, from the standpoint of cost and processing time, it is not practical for mass production. Therefore, we adopted a pre-tuning process involving plastic deformation to squeeze the beam port flange for mass production of the cavities for the SRILAC [10]. The rate of the frequency shift is about -20kHz/mm . The advantage of this method is that the process takes only one day and allows fine tuning. After the pre-tuning, helium jacket made of pure titanium was installed to the cavity.

PROTOTYPE CRYOMODULE

A schematic of the prototype cryomodule for the 75.5 MHz cavity is shown in Fig. 1. The length of the cryomodule, measured between the gate valves, was designed to be 1.34 m. Its total acceleration voltage was 2.9 MV with two QWRs. The SC cavity, whose beam ports are connected with bellows pipes and which is equipped with a fundamental power coupler (FPC) [12], is supported by 4 hollow pillars made of GFRP that are mounted on a common U-shape frame. The vacuum vessel is made of stainless steel (SUS304). The photos taken during cold mass assembly at the ISO class 1 clean room are shown in Fig. 7(A),(B),(C). To minimize heat conduction from the room-temperature part to the 4 K cold mass, a thermal shield is installed. The cavity is equipped with a magnetic shield made of μ -metal with a thickness of 1.5 mm, mounted on the helium jacket to cover the whole cavity (Fig. 7(E)). The thermal shield is cooled by a cryocooler (CH-110, Sumitomo Heavy Industries, Ltd.). Its cold head is connected to the bottom panel of the thermal shield with copper blades (Fig. 7(F)). The thermal shield provides thermal anchors to the beam pipes, power couplers, the cavity supports.

The cold part assembly, i.e., installation of the power couplers (Fig. 7(D)) to the cavity and the dummy, connection of the beam pipe bellows, and installation of a pair of gate valves at the two ends of the cryomodules (Fig. 7(A),(B),(C)), was completed in a ISO class 1 clean room prepared for the cryomodule assembly for the SRILAC cryomodules. The clean

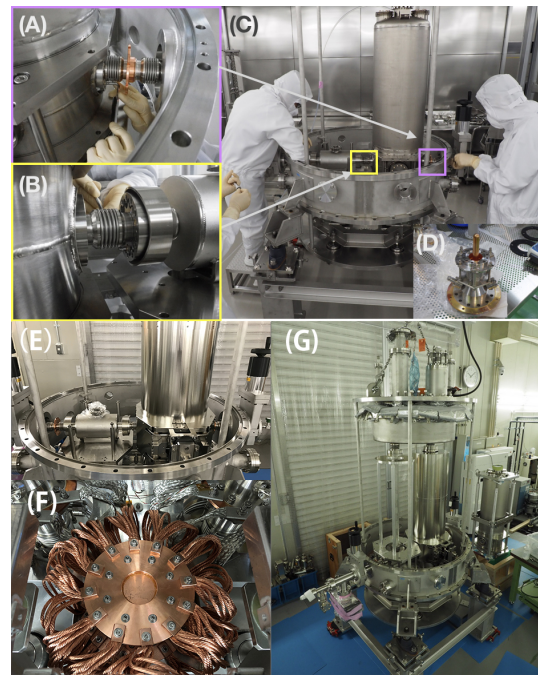


Figure 7: (A) Beam pipe bellows between cavities. (B) Beam pipe bellows at the end part. (C) Assembly work at ISO Class 1 clean room. (D) Power Coupler. (E) Assembly of tuner and local magnetic shield (μ -metal). (F) Connection between the head of the cryocooler and the bottom panel of the thermal shield. (G) Assembly of upper part of cryomodule.

room employed a KOACH fan filter unit with a guide screen, provided by KOKEN Ltd. [9]. The fan system is equipped with a nanofiber air filter and air flow control mechanism that generates coherent horizontal air flows. Ultrapure water is available inside the ISO class 1 clean room for cleaning of the parts.

After integration, the prototype cryomodule was moved and installed into the accelerator cave of the linac bldg. Then a cool-down test and RF test were performed. The prototype cavity was cooled to 4.2 K with liquid helium supplied from a 1000 L dewar. The bottom panel of the thermal shield was cooled to 46 K via copper blades connected to a cryocooler (Fig. 7(F)). The temperature of the top panel was 75 K.

The RF control system shown in Fig. 8 consists of a solid-state amplifier, transmission line with directional couplers (P_{in} , P_r), a fundamental power coupler, a cavity pickup (P_t), and a digital feedback module. A solid-state amplifier with

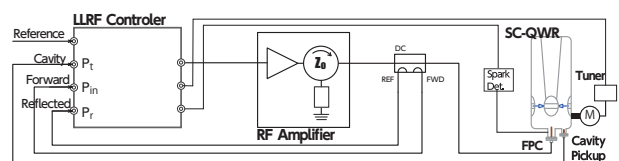


Figure 8: Block diagram of the RF control system.

a maximum output power of 4.5 kW and a digital feedback module, a low level RF (LLRF), have been developed, which excite the SC cavity with an external Q of 1×10^6 . The

Content from this work may be used under the terms of the CC BY 3.0 licence (© 2019). Any distribution of this work must maintain attribution to the author(s), title of the work, publisher, and DOI.

amplifier, whose output impedance is 50Ω , is capable of CW operation with open and short terminations in the absence of an external circulator.

A newly developed digital LLRF controller is dedicated to a system with a Q_{ext} as high as 1×10^6 . The system is based on a high-performance programmable logic chip FPGA. The cavity pickup signal and the signals from the directional couplers are digitized by harmonic sampling in sync with the 4/5 frequency of the reference signal (73.0 MHz). Converted digital signals are first demodulated to I-Q components, then converted to amplitude-phase components. The block diagram of the feedback control is shown in Fig. 9. Feedback control is performed with amplitude-phase components, and the feedback outputs are converted to I-Q and then the converted I-Q are processed with a modulator. DDS processes the RF signal according to the I-Q modulation.

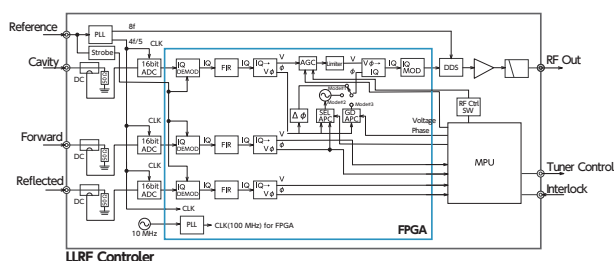


Figure 9: Block diagram of the digital feedback module.

An RF-on sequence must be built by considering a narrow bandwidth, Lorentz detuning, multipacting, and so on. The bandwidth is assumed to be 60 Hz. The Lorentz detuning Δf_L (Hz) is roughly proportional to the square of the accelerating gradient E_{acc} (MV/m) and its coefficient is about $-0.7 \text{ Hz}/(\text{MV/m})^2$. Multipacting occurs at an E_{acc} of $<0.1 \text{ MV/m}$, 0.4 MV/m and 0.9 MV/m . A block diagram of the RF-on sequence is shown in Fig. 10. The sequence utilizes the self-excited mode until the resonant frequency falls within the bandwidth, then the mode is switched to the generator-driven mode. In Fig. 11, the deviation of the power

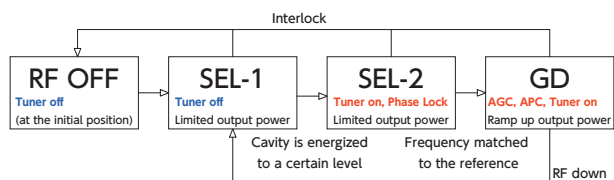


Figure 10: Block diagram of RF-On sequence.

level of the pickup signal (P_t/P_{t0}) was plotted as a function of the elapsed time during the 12-h operation test at an E_{acc} of 4.75 MV/m . The reliability for $|\Delta E_{\text{acc}}/E_{\text{acc}}| \leq 0.1\%$ was evaluated as 95%. Note that for this test, tuning was conducted manually by changing the frequency of the signal generator instead of moving the frequency tuner. The reliability will be improved by introducing the auto-tuner control.

Microphonics was observed in the phase error. To enhance the effect of the microphonics, the cryocooler for the thermal

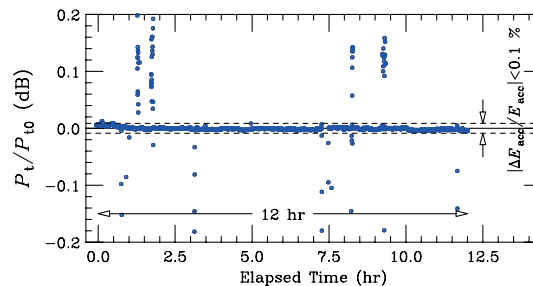


Figure 11: Power level of pickup signal (P_t) from SC cavity during a long-term operation test.

shield, whose support was designed so that the cryomodule is isolated from the vibration of the cryocooler, was tentatively mounted directly to the bottom of the cryomodule. As shown in Fig. 12, the phase of the cavity pickup signal showed a 40 Hz oscillation with a $\pm 1.5^\circ$ amplitude. A mechanical

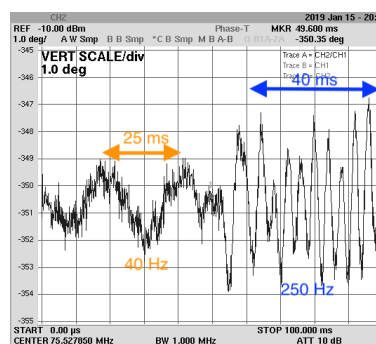


Figure 12: Microphonics appeared with a force oscillation by the cryocooler.

simulation predicted that the oscillation frequency was in the pendulum mode [6]. Furthermore, a faster oscillation of 250 Hz with an error of $\pm 3.5^\circ$ was observed. This might be due to the mechanical oscillation of the other part. When the cryocooler was turned off, these oscillations disappeared, but a phase oscillation with a frequency of 50 Hz and an amplitude of less than $\pm 1^\circ$ remained. For the SC-QWRs of the SRILAC, an extensive study on microphonics was conducted [13].

The frequency tuner changes the resonant frequency slightly by pushing the beam port flanges [6]. From the mechanical simulation its sensitivity to the length between the flanges is about -20 kHz/mm . The tuner, pneumatically driven by a motor located outside the vacuum chamber, tightens the cavity by a pair of surrounding wires (Fig. 13(A)) and then the gap length of the beam port was compressed along the beam axis, similarly to the tuner developed at ANL [14]. The shift in frequency induced by the tuner is limited to within -20 kHz because the maximum stress on the pure niobium part cannot exceed 90 MPa , as required by regulations for high pressure safety in Japan. A fast tuner is not installed since the 4.5 kW RF power (CW) is available with a bandwidth of $\pm 60 \text{ Hz}$.

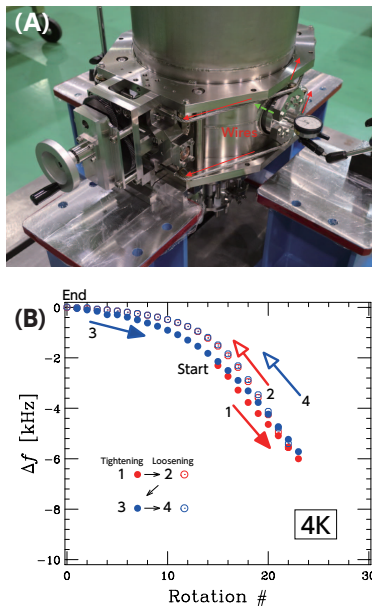


Figure 13: (A) Frequency tuner driven by a motor. A rotating handle was installed tentatively for an operation test. (B) Frequency shift vs number of rotations of the drive shaft handle.

The tuner test was performed after cool-down. The observed frequency shift is plotted in Fig. 13(B). Though a hysteresis was observed, it was acceptable from the standpoint of tuning control. The tuning range was limited presumably because of the mechanical loss of the driving system. The mechanical design was modified to minimize the mechanical loss of the tuner of the SRILAC.

SRILAC CRYOMODULE

The SRILAC cryomodule is based on a modified design of the first prototype cryomodule (Fig. 14). As a baseline for the cryomodule design, the beam vacuum and insulation vacuum are separated to prevent accumulation of particulates from the insulation vacuum. The operation temperature is 4 K. Modifications from the prototype cryomodule are tabulated in Table 2. The cryostat maintains the cold mass, which consists of 4 QWRs, a helium jacket, FPCs, magnetic shields, and dynamic tuner a 4.5 K with a 80 K shield. The focusing magnets with steering function, and the beam energy-position monitors are installed into the warm section outside the cryomodule. One of the most important issues in designing the beam transport line is the prevention of the contamination of SC cavities by particulates transported from the room-temperature section by the gas flow induced by the vacuum pressure gradient. To connect the different vacuum level parts and prevent gas flow into the high-vacuum section, a non-evaporable-getter-based differential pumping system is being developed [15].

The vacuum vessel made of carbon steel (SS400) reduces the background magnetic field to less than $12 \mu\text{T}$. Each of the QWRs is supported by 4 hollow pillars made of GFRP,

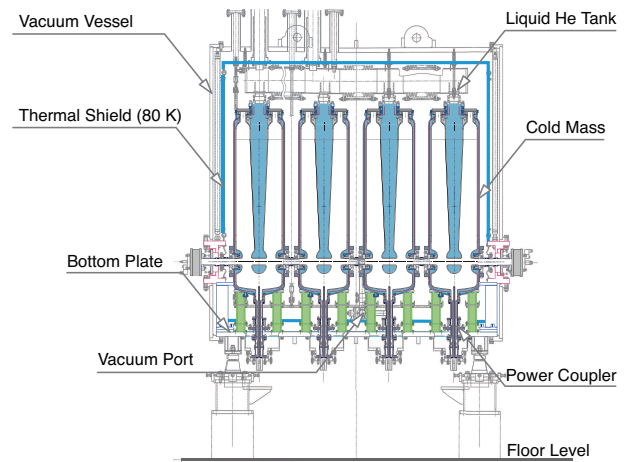


Figure 14: Schematic of SRILAC cryomodule.

Table 2: Cryomodule Specifications

Cryomodule	Prototype	SRILAC
Frequency	75.5 MHz (CW)	73.0 MHz (CW)
Operating Temp.	4 K	
# of cavities	2	4
Length	1337 mm	2200 mm
Focus Magnet	No	
Shape of Chamber	Cylinder	Cuboid
Chamber Material	SUS304	SS400
Thermal Shield	40 K	80 K
Local Mag. Shield	μ -metal	
	On the jacket	Inside the jacket
Cavity Int.	420 mm	430 mm
Static Load (4 K)	3.6 W	18 W
Cavity Support	Propping up structure	
Platform	Comm. Frame	Bottom Plate

which are mounted on a rigid bottom plate. The total static heat load is estimated to be 18 W, which consists of 6 W from FPC, 4.5 W through helium distribution pipes, 2.5 W from the driving shaft of tuners, and 2 W through the support pillars. For the SRILAC cavity, the local magnetic shield of μ -metal is encased inside the helium jacket, while the local magnetic shield was installed on the helium jacket for the 75.5 MHz prototype cavity. The advantages of this structure are that it enables to exclude the magnetic parts utilized for the tuner outside the shield and that it simplifies the construction of the cryomodule assembly.

For the power coupler, a new design was introduced. While the coupler for the first prototype SC-QWR is based on a double window structure [12], the new design employed a single warm window structure, as shown in Fig. 15(A). The disadvantage of the single window structure might be the difficulty of handling the long antenna, with a length of about 30 cm. On the other hand, owing to the simple structure of the single window coupler, it is much easier to fabricate than the double window type. Cleaning and drying before installation into the cavity are also easier. After fabri-

Content from this work may be used under the terms of the CC BY 3.0 licence (© 2019). Any distribution of this work must maintain attribution to the author(s), title of the work, publisher, and DOI.

ation, 5 pairs of couplers are cleaned, conditioned with a test resonator (Fig. 15(B)) and installed into the cavities in the ISO class 1 clean room at RIKEN.

So far, 10 QWRs were fabricated [10] with fundamental power couplers and integrated into 3 cryomodules. The cryomodules for the SRILAC were transferred to the linac bldg., where the final assembly (Fig. 16(A)) was built and the installation and alignment were performed (Fig. 16(B)). The liquid helium delivery lines were connected with U-tubes to the cold valve box of the helium transfer line (Fig. 16(C)). Details of the construction status have been reported in [15].

SUMMARY AND PERSPECTIVES

At RIKEN RIBF, development of SC-QWRs for the heavy-ion linac started in 2013. With the first prototype cavity (75.5 MHz), an extensive study was conducted on surface treatment, and the cavity yielded a Q_0 of 2×10^9 at $E_{acc}=4.5$ MV/m. The cavity was integrated into the prototype cryomodules. A cool-down test and RF test were performed with the prototype cryomodule using the newly developed LLRF system and a solid-state amplifier.

The RIKEN heavy ion linac will have an acceleration voltage and intensity upgrade upon the introduction of an SC linac based on high-performance SC-QWRs and an SC-ECR ion source. The prototype cavity of the SRILAC with a frequency of 73 MHz, which had some modification from the first prototype SC-QWR (75.5 MHz), was fabricated and tested. Its performance was successfully improved as

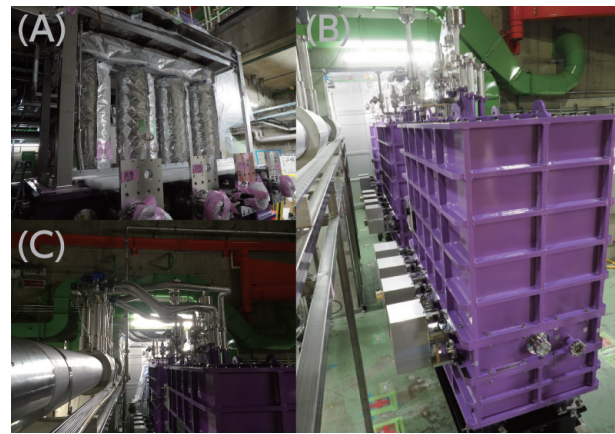


Figure 16: (A) Cryomodule in the final assembly, (B) Cryomodules after alignment, (C) U-tubes were connected between the cryomodule and the transfer line.

$Q_0=3.4 \times 10^9$ at $E_{acc}=6.8$ MV/m. Ten SC-QWRs were fabricated and processed following the recipe for the prototype. All the SC-QWRs showed almost comparable performances in terms of the prototype cavity for the SRILAC. After the acceptance test, the SC-QWRs were integrated into three cryomodules. The cryomodules have already been installed into the accelerator cave of the linac bldg., aligned to the existing beam line and connected to the helium transfer line. The construction of a control system is underway, and the first cool-down test with a helium refrigerator has been scheduled for August, 2019 [15].

ACKNOWLEDGEMENTS

This work was funded by the ImPACT Program of the Japan Council for Science, Technology and Innovation (Cabinet Office, Government of Japan). The authors are grateful to Dr. A. Kasugai of QST Rokkasho and Prof. K. Saito of FRIB/MSU for technical discussions on the design of the cavity and on assembly work.

REFERENCES

- [1] H. Okuno *et al.*, *Prog. Theor. Exp. Phys.*, vol. 2012, no. 1, pp. 03C002, 2012.
- [2] M. Odera *et al.*, *Nucl. Instrum. Methods A*, vol. 227, p. 187, 1984.
- [3] K. Suda *et al.*, *Nucl. Instrum. Methods A*, vol. 722, p. 55, 2013.
- [4] K. Yamada *et al.*, “Conceptual Design of SC Linac of RIBF Upgrade Plan”, in *Proc. SRF’13*, Paris, France, Sep. 2013, paper MOP021, p. 137.
- [5] <http://www.jst.go.jp/impact/en/program/08.html>
- [6] N. Sakamoto *et al.*, “Design Studies for Quarter-Wave Resonators and Cryomodules for the Riken SC-LINAC”, in *Proc. SRF’15*, Whistler, Canada, Sep. 2015, paper WEBA06, pp. 976–981.
- [7] <http://www.cst.com>

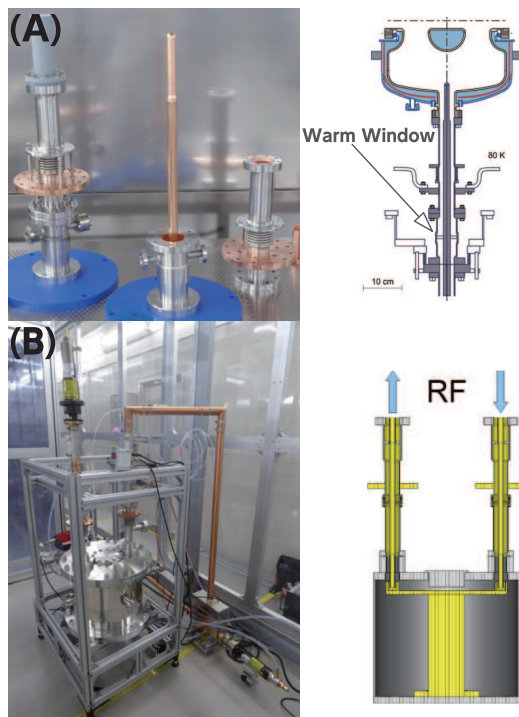


Figure 15: (A) Single window power coupler developed for the SRILAC. (B) 5 pairs of power coupler were conditioned with 5 kW RF power using a test chamber.

- [8] N. Sakamoto *et al.*, “Construction and Performance Tests of Prototype Quarter-wave Resonator and Its Cryomodule at RIKEN”, in *Proc. SRF’17*, Lanzhou, China, Jul. 2017, pp. 681–685. doi : 10.18429/JACoW-SRF2017-WEYA02
- [9] A. Miyamoto, H. Hara, K. Kanaoka, K. Okihira, K. Sennyu, and T. Yanagisawa, “MHI’s Production Activities of Superconducting Cavity”, in *Proc. SRF’15*, Whistler, Canada, Sep. 2015, paper THPB029, pp. 1141–1145.
- [10] K. Suda *et al.*, “Fabrication and Performance of Superconducting Quarter-Wavelength Resonators for SRILAC”, presented at the SRF’19, Dresden, Germany, Jun.-Jul. 2019, paper MOP055, this conference.
- [11] L. Popielarski *et al.*, “Process Developments for Superconducting RF Low Beta Resonators for the ReA3 LINAC and Facility for Rare Isotope Beams”, in *Proc. LINAC’12*, Tel Aviv, Israel, Sep. 2012, paper MOPB071, pp. 342–344.
- [12] K. Ozeki *et al.*, “Design of Input Coupler for RIKEN Superconducting Quarter-Wavelength Resonator”, in *Proc. SRF’15*, Whistler, BC, Canada, Sep. 2015, paper THPB084, p. 1335.
- [13] O. Kamigaito, K. Ozeki, N. Sakamoto, K. Suda, and K. Yamada, “Measurement of Mechanical Vibration of SRILAC Cavities”, presented at the SRF’19, Dresden, Germany, Jun.-Jul. 2019, paper TUP042, this conference.
- [14] P. N. Ostroumov *et al.*, “Development of Compact Cryomodules Housing HWRs for High-intensity SC CW Linacs”, in *Proc. SRF’13*, Paris, France, Sep. 2013, paper MOP066, pp. 277–279.
- [15] K. Yamada *et al.*, “Construction of Superconducting Linac Booster for Heavy-Ion Linac at RIKEN Nishina Center”, presented at the SRF’19, Dresden, Germany, Jun.-Jul. 2019, paper TUP037, this conference.